Ultrasonics 97 (2019) 29–37

Contents lists available at ScienceDirect

Ultrasonics

journal homepage: www.elsevier.com/locate/ultras

A high-resolution structural health monitoring system based on SH wave piezoelectric transducers phased array

Qiang Huan[a,b], Mingtong Chen[a,b], Zhongqing Su[c], Faxin Li[a,b,d,*]

[a] LTCS and College of Engineering, Peking University, Beijing 100871, China
[b] Center for Applied Physics and Technology, Peking University, Beijing, China
[c] Department of Mechanical Engineering, The Hong Kong Polytechnic University, Hong Kong Special Administrative Region
[d] Beijing Key Laboratory of Magnetoelectric Materials and Devices, Peking University, Beijing, China

ARTICLE INFO

Keywords:
Structural health monitoring
Phased array
Shear horizontal wave
Guided wave
Piezoelectric transducer

ABSTRACT

Guided wave based structural health monitoring (SHM) has been regarded as an effective tool to detect the early damage in large structures and thus avoid possible catastrophic failure. In recent years, Lamb wave phased array SHM technology had been intensively investigated while the inherent multi-mode and dispersive characteristic of Lamb waves limits its further applications. In comparison, the fundamental shear horizontal (SH_0) wave is non-dispersive with uncoupled displacements and thus more promising for defect detection. In this work, we proposed an SH_0 wave linear phased array SHM system based on our recently proposed omni-directional SH wave piezoelectric transducer (OSH-PT). Firstly, the working principle of the phased array system was presented and the total focusing method (TFM) was employed for imaging. Then the SH_0 wave mode generated by the OSH-PT was confirmed in a defect-free plate. Finally, experiments were carried out to examine the performances of this SHM system. Results showed that the proposed system can detect a through-thickness hole as small as 2 mm in diameter with the location error only about 6.3 mm. Moreover, the proposed phased array system can also detect multi-defects. Due to its low working frequency and thus low attenuation, the proposed phased array system is capable of monitoring large structures. This work will lay the foundations of SH wave based phased array SHM.

1. Introduction

The integrity of large structures is always an important issue in engineering fields such as aerospace, chemical and civil engineering, as the possible catastrophic failure could cause huge loss in both casualty and economic. Structural health monitoring (SHM) is regarded as an effective tool to prevent these events and has been under rapid development in recent years [1,2]. By building SHM systems, the status of structures can be under real-time monitoring even during its service period. When sudden or gradual changes happened, the possible damage in structures can be quickly located and quantified. Then, condition-based maintenance policies can be taken to reduce the risk of failure and prolong its service life [3].

Among the existing SHM methods, guided wave based technology is more promising for its less attenuation and thus long distance/large area coverage [4]. In practical applications, transducer arrays are commonly used because single transducer can hardly provide enough information for defects localization. The employed transducer array is usually classified into two types: sparse array and phased array. For the sparse array system, transducers were bonded on the structures with certain distance, dividing the monitoring area into many subareas. Intensive works had been done on the sparse array based SHM method [5–7] and many signal processing techniques [8–10] were successively proposed to increase its detecting capability. However, a baseline in healthy condition is usually required for a sparse array SHM system, which is easily influenced by external factors such as temperature variations. Although some strategies have been proposed to compensate the variations of the baseline [11,12], it will always be a problem in practical applications. In addition, the sensors have to overspread the whole structure in a sparse array system, which may not be feasible in some cases.

In comparison, phased array systems do not need to build sensor networks all over the structure since the B-scan detecting method can easily realize full area inspection. More importantly, it can detect defects without baseline. Many researchers had investigated the capability of the phased array system in damage detecting. Wooh and Shi studied

* Corresponding author at: LTCS and College of Engineering, Peking University, Beijing 100871, China.
E-mail address: lifaxin@pku.edu.cn (F. Li).

https://doi.org/10.1016/j.ultras.2019.04.005
Received 21 February 2019; Received in revised form 28 April 2019; Accepted 28 April 2019
Available online 29 April 2019
0041-624X/

the beam steering characteristics of linear phased arrays ultrasonics [13,14]. Wilcox et al. employed circle-shaped electromagnetic acoustic transducer (EMAT) arrays to inspect large metallic plates [15]. Giurgiutiu and Bao proposed the concept of in situ SHM for thin-wall structures by using linear piezoelectric transducer arrays [16]. Yu and Giurgiutiu then systematically investigated piezoelectric transducer based phased array in configurations, parameter optimization and signal processing [17–20]. Piezoelectric transducer based phased array SHM had been successfully applied in isotropic plates and then extended to layer composites [21,22]. Despite of above-mentioned success, the inherent multi-modes and dispersion of the employed Lamb waves have strictly limited the further development of current phased array SHM [23]. Although these demerits can be reduced by strategies like turning frequency [24], they can never be completely avoided.

In plate-like structures, there only exists one wave mode that is totally non-dispersive, i.e., the fundamental shear horizontal (SH_0) wave. In actual applications, omni-directional transducers are preferred for phased array systems. However, unlike Lamb waves which can easily be generated and received omni-directionally by piezoelectric wafers, the omni-directional generation and reception of SH_0 wave using piezoelectrics is always a challenge. Borigo et al. proposed a design of omni-directional SH wave piezoelectric transducer (OSH-PT) based on two circumferentially poled half-rings [25] but no experimental results were provided. Meanwhile, it should be noted here that the uniform circumferential poling is not possible to realize in practice. Belanger et al. [26] and Miao et al. [27] developed the OSH-PT by synthesizing circumferential poling based on thickness-shear d_{15} mode and face-shear d_{24} mode PZT wafers, respectively. The sensitivity variations along different directions for these two types OSH-PTs are about 20% and 15%, which are acceptable but not desirable. Huan et al. proposed an OSH-PT with excellent performances based on thickness-poled, thickness-shear d_{15} mode PZT ring consisting of twelve elements [28]. This OSH-PT was recently employed in a variable-frequency sparse array SHM system whose performances are superior to the Lamb wave based counterparts [29]. More recently, this OSH-PT was optimized to be two half-rings based, which is more promising in practical SHM applications where a large number of OSH-PTs are required [30].

So far, SH wave based phased array system has never been investigated. Thus in this work, we aimed at developing a SH wave based phased array SHM system using our proposed two half-rings based OSH-PT [30]. Firstly, the working principle of the phased array SHM system and the employed total focusing method (TFM) imaging algorithm [31] were presented. Then the SH_0 wave mode generated by the OSH-PT was confirmed in a defect-free aluminum plate. Finally, the performances of the SH_0 wave phased array SHM system were examined on an aluminum plate with surface defects and through-thickness holes. Results indicated that the proposed SHM system can effectively detect a through-thickness hole with the diameter as small as 2 mm and the location error is only 6.3 mm. Besides, it can detect multi-defects simultaneously. This work may pave the way for SH wave based phased array SHM.

2. Principle

Firstly, the working principle of the proposed SH wave phased array system was introduced. The system was a linear phased array that consists of N thickness-poled half-ring based OSH-PTs, as shown in Fig. 1. The configuration, fabrication and performance of this OSH-PT can be found in our recent work [30]. Each OSH-PT was regarded as a point-like transducer with omni-directivity. The spacing between the adjacent OSH-PTs was d. In this work, we employed the total focusing method (TFM) for imaging [31]. The signals were collected in a round-robin fashion that one element was used as the actuator while the others were served as sensors. In this way, $N \times (N-1)$ pairs of signals will be collected for each scan. It should be noted that the signals generated and received by the same transducer was not included here. This is because this type signal was collected using a diplexer and the received signal is apt to be influenced by the drive signal if the attenuation was not well adjusted. Note that the collected $N \times (N-1)$ pairs of signals were enough for the proposed system to locate the defect.

Beamforming of the proposed system was based on the principle of constructive interference. Due to the spacing of transducers, the distance between one transducer and the target point was different from others. Thus, different time delay was needed for different pairs of transducers in order to realize constructive interference. Here, the parallel ray approximation was employed to calculate the distance difference. This algorithm takes the far field approximation and plane wave front that the distance between the transducer and the target r is much larger than the transducer spacing d i.e. $r \gg d$ and the wave would propagate with a plane wave front. Within the near field, the results may contain large errors which can be avoided by adopting exact wave propagating path [32]. Because of the mirror symmetry, this linear phased array cannot differentiate between defects on opposite sides of the linear array. With regard to a target point X at azimuth θ, the propagating distance for the mth OSH-PT was shortened by $m(d\cos\theta)$ in comparison with the reference signal, as shown in Fig. 1. This signal will then arrive at target X earlier by

$$\Delta tm = md\cos\theta/v_g \tag{1}$$

Here, v_g is the group velocity of the employed wave mode. Note that in this work, we employed the non-dispersive SH_0 wave whose group velocity is constant and equal to the bulk shear wave velocity of the waveguide. Thus the time delay of this phased array system is independent of the working frequency and thickness of the waveguide, which is obviously superior to the Lamb wave based systems [16–19].

The simplest way to achieve constructive interference in wave generation is to apply individual time delays for corresponding OSH-PTs, then the total signal received at point X will be

$$S_{X-\text{generation}}(t, \theta) = \sum_{m=0}^{m=N-1} s_{m\to X}(t - \Delta t_m) \tag{2}$$

For the wave reception, if the point X was served as the source, the signal received by the mth OSH-PT will also arrive earlier by $\Delta t_m = md\cos\theta/v_g$. The received signals achieved constructive interference by delaying the time as

$$S_{X-\text{reception}}(t, \theta) = \sum_{m=0}^{m=N-1} s_{X\to \text{m}}(t - \Delta t_m) \tag{3}$$

Since the proposed system worked in the pulse-echo way i.e. the time delaying was needed to be considered for both wave generation and reception. Thus, the final signal would realize beamforming via

$$S_X(t, \theta) = \sum_{\substack{i=0 \\ i\neq j}}^{N-1} \sum_{j=0}^{N-1} s_{i\to j}(t - \Delta t_i - \Delta t_j) \tag{4}$$

With the rotation of θ, B-scan was realized in the whole inspection area for damage inspection.

3. Experimental

Experiments were carried out on a 1200 × 1200 × 2 mm aluminum plate to examine the performances of the proposed phased array system in defect inspection. The experimental setup was shown in Fig. 2(a), where nine thickness-poled half-ring based OSH-PTs named T_1–T_9 were bonded on the aluminum plate to construct the linear phased array. The position of the central transducer T_5 was (600 mm, 600 mm) and the spacing between the adjacent OSH-PTs was 15 mm. Each OSH-PT was 12 mm in outer diameter, 6 mm in inner diameter and 2 mm in thickness with the material of PZT-5H. Bearing in mind that shear wave velocity of aluminum is 3100 $m{\cdot}s^{-1}$ and based on the $\lambda/2$ element

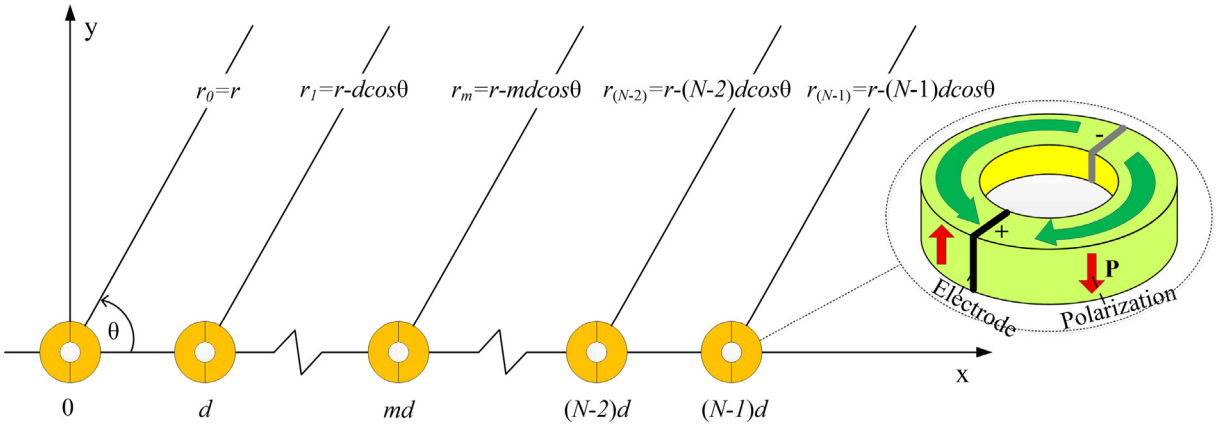

Fig. 1. The principle of the OSH-PTs based SH wave phased array system.

spacing criterion [33], to avoid the grating lobes along all directions, the working frequency of this phased array system should be lower than 103 kHz. However, according to our recent work [30], the employed OSH-PT here has good performances in SH wave excitation/reception and Lamb waves suppression above 120 kHz. The excited SH_0 wave to Lamb waves ratio (SLR) is above 20 dB in most frequency range from 120 kHz to 250 kHz and can even reach 25 dB when frequency is near 140 kHz. In this work, to suppress the grating lobes at large steering angles above 103 kHz, all the transducers were excited by a five-cycle Hanning window-modulated sinusoid tone burst [33]. In this way, only at the desired steering angle, all tone bursts would appear at the same time point with same phase, realizing the strongest constructive interference. For other steering angles, the tone bursts would not appear at the same time point, resulting in weaker constructive interference even if their phase difference corresponds to integer times of the central-frequency wavelength. Thus, the grating lobes can be effectively suppressed by using tone burst drive signals.

In order to validate the feasibility of the proposed phased array system in defect detecting, firstly, an iron rod with 20 mm in diameter and 100 mm in length was bonded on the plate to simulate a surface defect named D_1. After collecting all the $N \times (N-1)$ pairs of signals, the glued iron rod was removed and a 2 mm-diameter through-thickness hole was introduced at the same position as another type of defect. Then all the $N \times (N-1)$ pairs of signals were collected again. Next, this 2 mm hole was expanded to 4 mm in diameter and then to 6 mm in diameter. At each step, all the $N \times (N-1)$ pairs of signals would be collected again. Finally, another 6 mm through-thickness hole named D_2 was introduced to examine the capability of the proposed system in multi-defects detection. The position of all defects was illustrated in Fig. 2(a) and also shown in the photo of the experimental setup, i.e., Fig. 2(b). During testing, the exciting signal of five-cycle Hanning window-modulated sinusoid tone burst was generated by a function generator (3320A, Agilent, USA) and amplified by a power amplifier (KH7602M). The amplitude of the drive voltage was fixed at 120 V for all the testing. An oscilloscope (Agilent DSO-X 3024A) was used to collect the signals received by the sensors with 128 times trace averaging.

Firstly, the group velocity of the excited wave was measured in a defect-free aluminum plate to validate the single-mode SH_0 wave. Two OSH-PTs with the distance of 360 mm were used as a pair of actuator and sensor. The excitation and reception performances at 120 kHz and 180 kHz were tested and the results were shown in Fig. 3. It can be found that at both frequencies, there only appeared one waveform in the received signal, as shown in Fig. 3(a) and (b). After employing continuous wavelet transform (CWT), it can be clearly found that the internal time between the drive and received signals was 117.2 μs and 115.6 μs respectively, corresponding to wave velocities of 3072 $m \cdot s^{-1}$ and 3114 $m \cdot s^{-1}$. This result is in good agreement with the group

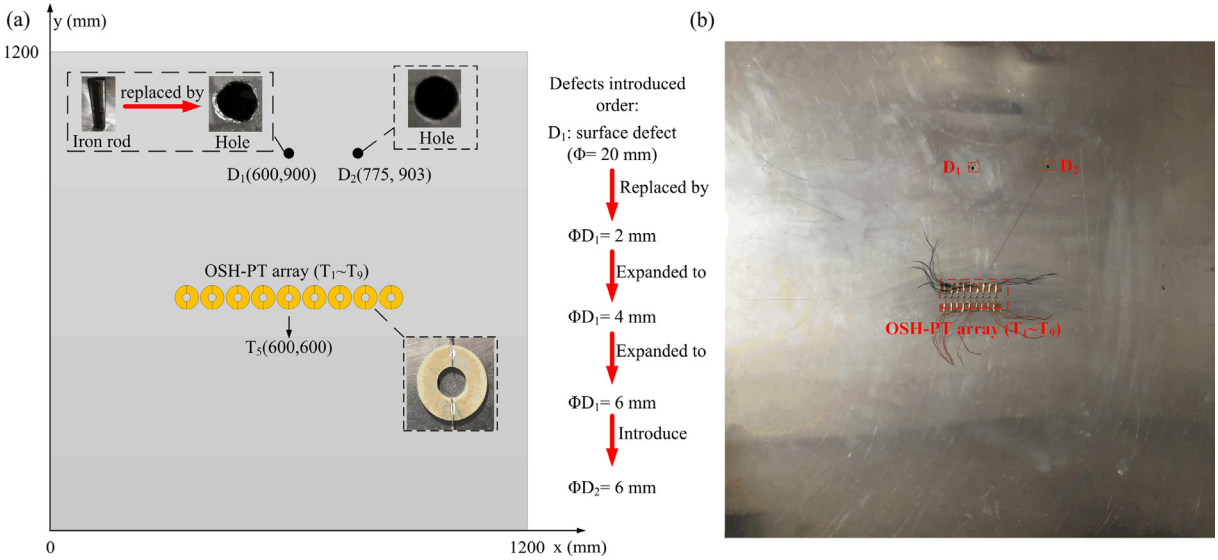

Fig. 2. Experimental setup of the OSH-PT based phased array system. Nine OSH-PTs (named T_1–T_9) were bonded on a 2 mm-thick aluminum plate to form a linear phased array and two defects (named D_1 and D_2) were introduced sequentially. (a) Schematics; (b) Photo.

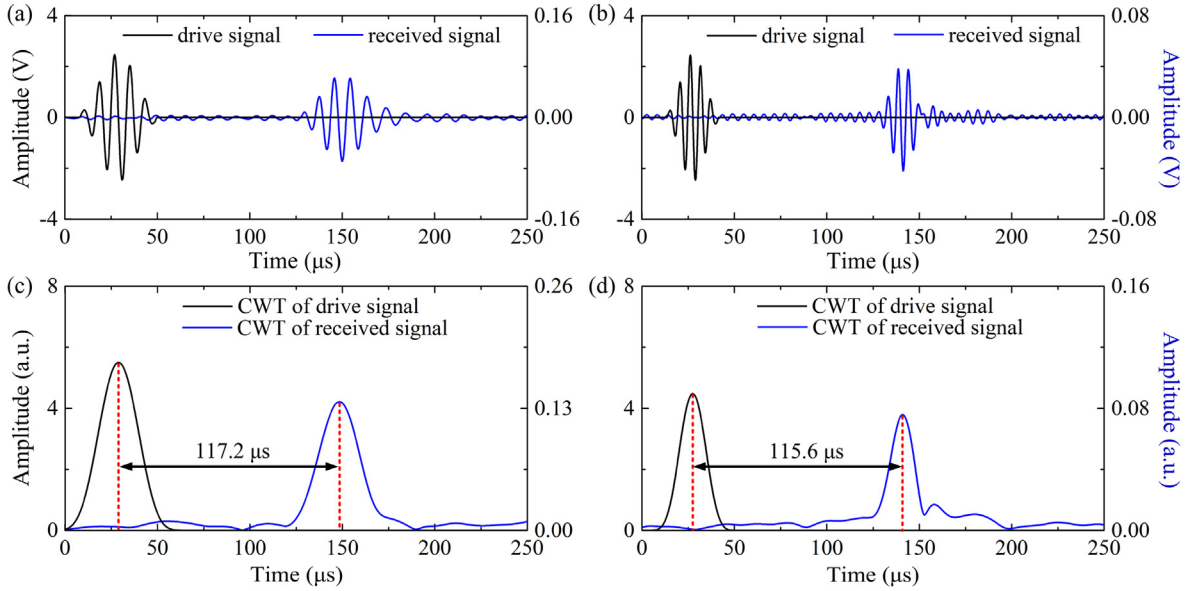

Fig. 3. Signals excited and received by a pair of OSH-PTs at (a) 120 kHz and (b) 180 kHz. (c) and (d) Were continuous wavelet transform (CWT) of the drive signal and received signal.

velocity of SH_0 wave (or the bulk shear wave velocity) of 3100 $m{\cdot}s^{-1}$ in an aluminum plate. Hence it can be confirmed that single mode SH_0 wave was excited in the proposed phased array system.

4. Results and discussions

4.1. Surface defect detection

Fig. 4 presented an example of signal reconstruction for the surface defect i.e. glued iron rod at D_1 location by the SH_0 wave phased array system. Here the working frequency was set to be 145 kHz as the excited SH wave to Lamb waves ratio (SLR) by the transducer is relatively large around this frequency [30]. It can be seen from Fig. 4(a) that the original signal received by one OSH-PT included three parts: initial bang, echoes reflected from the defect and from boundary. The initial bang consists of the signal directly propagating from the actuator to the sensor and the reflections between them. These signals were useless and would be cut-off in signal processing. The boundary reflection would also be removed in signal processing. For the echo from the defect, its amplitude was rather small and easily masked by the noise, as plotted in Fig. 4(a). It is almost impossible to determine the position of the defect directly using this kind of signal. After adopting the TFM to process all the signals, the amplitude of the reconstructed echo from the defect was greatly enhanced, as shown in Fig. 4(b). This is because the echoes from the defect realized constructive interference after the TFM processing while the random noise was not enhanced significantly. Thus the enhanced amplitude of the echo was much larger than that of the noise, resulting in an identifiable wave package in the reconstructed signal.

The capacity of the proposed phased array system in detecting a surface defect i.e. glued iron rod was firstly examined at 145 kHz. The reconstructed signals at 30°, 60° and 90° (the defect direction) were plotted in Fig. 5(a), (b) and (c) respectively for comparison. It can be seen that at the direction without defect i.e. 30° and 60°, there is no identifiable wave package of the echo in the reconstructed signal. Only at 90° direction where the defect is located, an identifiable wave package appeared in the reconstructed signal due to the constructive interference of the reflected echoes from the defect. At other directions, the echoes would interfere in a chaotic way. After fixing the direction of the defect, further signal processing can be employed to determine its position, as shown in Fig. 5(d)–(f). Firstly, the continuous wavelet transform (CWT) was adopted to analyze the reconstructed signals. Here, t_a was the ending time of the initial bang and t_b was the starting time of the boundary reflection, which was only determined by the experimental system itself. The signal before t_a and after t_b would be removed in defects inspection. The effective signal for defects

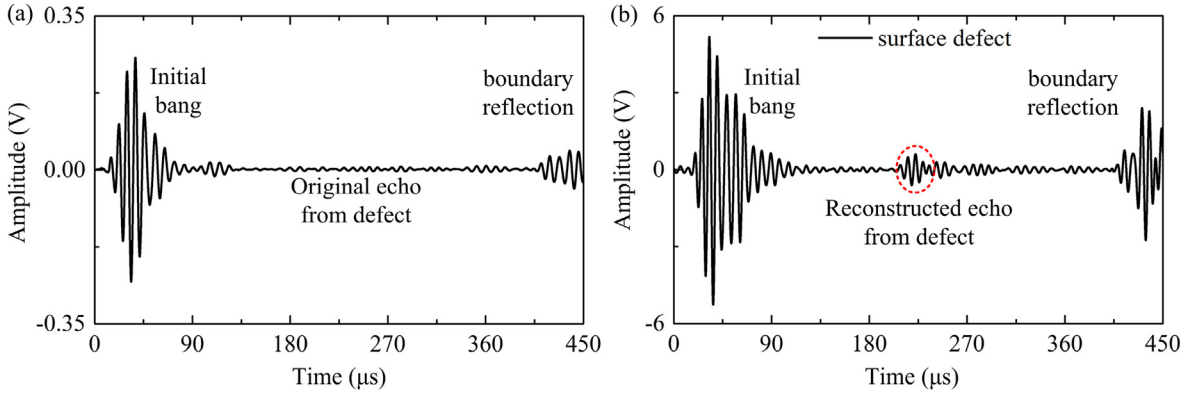

Fig. 4. The example of signal reconstruction at 145 kHz for a surface defect by the SH_0 wave phased array system. (a) Original signal received by one OSH-PT; (b) reconstructed signal after constructive interference of all OSH-PTs.

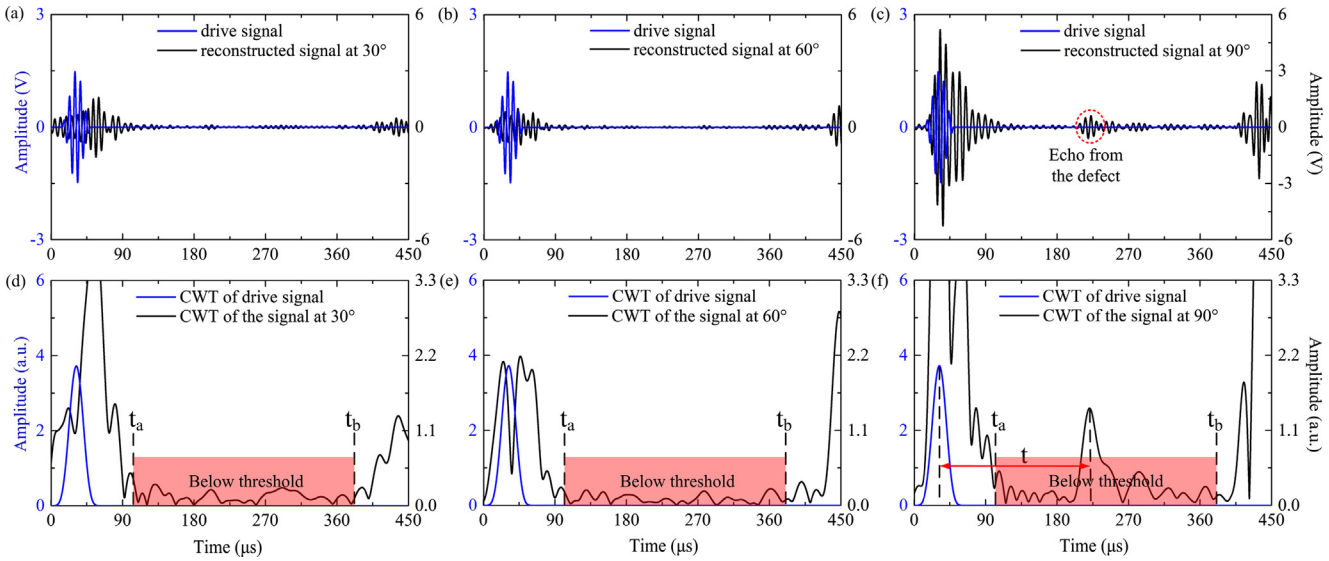

Fig. 5. The reconstructed signals at (a) 30°, (b) 60° and (c) 90° direction of the linear array for the surface defect was at 145 kHz. (d), (e) and (f) were the corresponding signals after continuous wavelet transformation (CWT).

localization was that between t_a and t_b. Then, threshold truncation was applied to remove the background noise. It can be found that with setting threshold value to be 50% of the maximum amplitude, all noise can be removed and only one wave package at 90° direction remained which corresponds to the defect. The drive signal was also plotted here to determine the time interval t between the phased array system and the defect. Thus, the position of the defect can be determined.

It should be noted that tradeoff should be made when choosing the suitable threshold value. If using a lower threshold value, more information would remain in the reconstructed signals. But the background noise may not be totally removed in this case. While if adopting a high threshold value, some useful information may be cut off as noise, leading to missed detection.

Because of the initial bang, there exists a blind zone around the transducer array that the artifacts are in high intensity. Similarly, the boundary reflection restricts the maximum detecting distance of the proposed phased array system. Hence, the inspection area of the proposed system was a ring area. This can be clearly seen in Fig. 6(a) which is the imaging result for the 20 mm surface defect at 145 kHz. The blind zone caused by the initial bang was enclosed by the marked inner circle and that caused by the boundary reflection was outside of the marked outer circle, as the grey zone plotted in Fig. 6. The effective detecting zone should be the ring area between the two circles. However, it should be pointed out that due to the reverberation of signals between transducers, the amplitude of the echoes from defects may decrease significantly, reducing the detecting capability of the proposed system along array orientation (0° and 180°). Meanwhile, the imaging result in the near field may contain large errors, as mentioned in Section 2, which can be avoided by adopting exact wave propagating path [32]. It can be seen from Fig. 6(a) that there appeared two highlight areas which are mirror symmetric. One is the actual position of the defect (up), the other is the mirrored artifact (bottom) which is caused by the mirror symmetry of the linear phased array using omnidirectional transducers and it cannot be avoided. Thus in the rest of the paper, only half plate was presented for the imaging results. Despite of this, the proposed system can detect the surface defect effectively. The located defect position was (594 mm, 893 mm), which is very closed to its actual position (600 mm, 900 mm) with the location error about 9 mm. This location error was mainly caused by the surface defect itself due to its size of 20 mm in diameter. Compared with the large detecting area, this level of location error can be negligible. Fig. 6(d) presented the threshold truncation result of Fig. 6(a). Throughout the paper, the threshold value was set to be 50% of the maximum amplitude, which is considerably smaller than that of 80% in Lamb wave based phased array system [17]. From Fig. 6(d), it can be found that all background noise was successfully removed, indicating the better performance of the proposed SH_0 wave phased array system.

The imaging result of the surface defect at 100 kHz were presented in Fig. 6(b), from which it can be seen that even at 100 kHz, the proposed system can also detect the defect but there appeared some artifacts near the near-field zone, which cannot be fully removed after 50% threshold truncation, as seen in Fig. 6(e). The main cause of these artifacts was the undesirable performance of the transducer at 100 kHz and thus unsatisfied received signals. With the rise of operating frequency, the system can detect the defect more accurately and the artifacts gradually faded away. The imaging result at 175 kHz was plotted in Fig. 6(c) and the result after 50% threshold truncation was plotted in Fig. 6(f), from which it can be seen that the surface defect can also be clearly detected. Furthermore, from all the subfigures in Fig. 6, it can be found that the image amplitude corresponding to the defect decreased with the increasing frequency. This was mainly caused by the rising attenuation at higher frequency [34] and the transducer's frequency response. Referring to the signal-to-noise ratio curve of the OSH-PT in SH wave generation/reception which was plotted in our previous work [30], to get better imaging results, the operating frequency was set to be 145 kHz in the rest of this paper. Note that the Lamb wave phased array systems have to work at a fixed frequency in order to realize quasi-single wave mode [24]. In comparison, the proposed SH_0 wave phased array can detect the defects at varied frequencies, which has obvious advantages in detecting different-sized defects.

4.2. Single through-thickness defect

After validating the capability of the proposed phased array system in surface defect detection, the glued iron rod was removed and a through-thickness hole with the diameter of 2 mm, 4 mm and 6 mm was introduced at the same position in sequence. The reconstructed signals for the holes at 145 kHz were presented in Fig. 7. It can be seen from Fig. 7(a) that even for the 2 mm hole, the reconstructed echo from the defect was still identifiable although its amplitude was very small. In comparison, the amplitude of the reconstructed echo for the 4 mm hole and 6 mm hole was much higher, as plotted in Fig. 7(b) and (c). This is easy to understand since a larger defect will cause stronger reflection. This result also implied that it is easier to detect a large defect than a

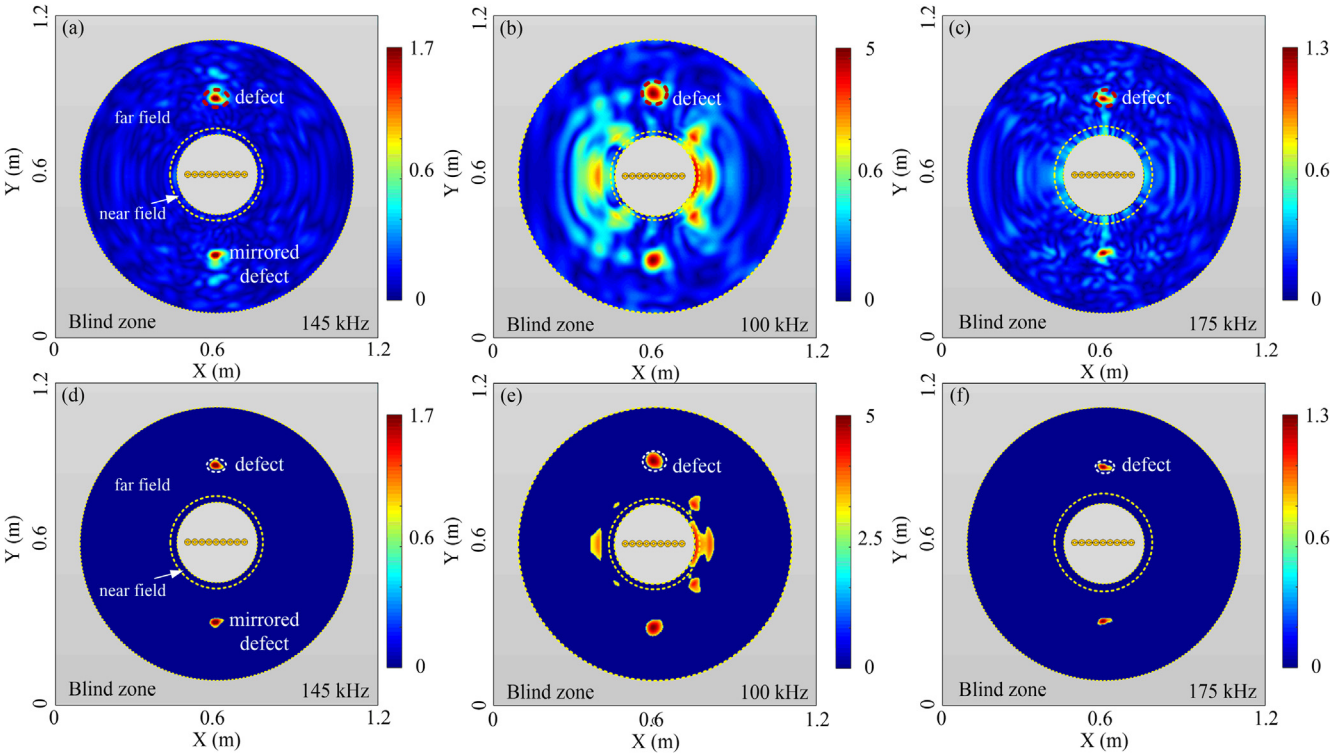

Fig. 6. The imaging results for the surface defect at 145 kHz (left), 100 kHz (middle) and 175 kHz (right). Up: Original results. Bottom: Results after threshold truncation (50% of the maximum amplitude).

smaller one.

Fig. 8(a)–(c) presented the original imaging results for the single through-thickness hole with the size of 2 mm, 4 mm and 6 mm at 145 kHz. For the 2 mm hole case in Fig. 8(a), it can be seen that one highlight area corresponding to the hole appeared in the reconstructed image with small artifacts around, which indicated that the proposed phased array system can detect a 2 mm through-thickness hole 300 mm away. The high resolution in defect inspection was benefited from the single mode non-dispersive SH_0 wave employed in the proposed system. As expected, when the size of the hole was expanded to 4 mm and 6 mm, the imaging amplitudes corresponding to the defects were obviously enhanced, as plotted in Fig. 8(b) and (c), and the artifacts faded away due to its low relative amplitude. The imaging results for the 2 mm, 4 mm and 6 mm hole after 50% threshold truncation were plotted in Fig. 8(d), (e) and (f), respectively, from which it can be seen that the artifacts can be totally removed for the 4 mm and 6 mm hole cases. While for the 2 mm hole, the small artifacts still exist in Fig. 8(d) and it can be removed if a higher threshold value was used. Thus, we inferred that the 300 mm away, 2 mm-diameter through-thickness hole may be the detection limit of this SH_0 wave phased array system.

The location results for the through-thickness hole with different diameter at 145 kHz were listed in Table 1. It can be seen that the location error is about 6.3 mm for the 2 mm-hole, 5.1 mm for the 4 mm-hole and only 2.2 mm for the 6 mm-hole. The decreased location error corresponding to the larger hole was also attributed to the increased amplitude of the reconstructed echo. From all the results above, it can be concluded that the proposed phased array system can detect both surface defects and through-thickness defects in high resolution.

A simple comparison was conducted to illustrate the difference of the proposed system in detecting different types of defects. The reconstructed signals at 145 kHz for the 20 mm surface defect and the 4 mm through-thickness hole were presented in Fig. 9(a) and (b) respectively. By locally amplifying the echoes, it can be found that the amplitudes for these two defects was nearly the same although their sizes were quite different. That is, a 20 mm surface defect is almost equivalent to a 4 mm-hole as far as the wave reflection is concerned. This is due to the fact that the vibration mode of the SH_0 wave is in-plane. The adhesive interface i.e. the surface defect, was a weak interface for SH_0 wave reflection because the wave can still propagate through this defect zone. In comparison, the interface resulted by a through-thickness hole will cause very strong SH_0 wave reflection since the wave can no longer propagate through this defect zone. Thus, for the proposed SH wave based phased array system, it is more difficult to detect a surface defect than a same-sized through-thickness defect.

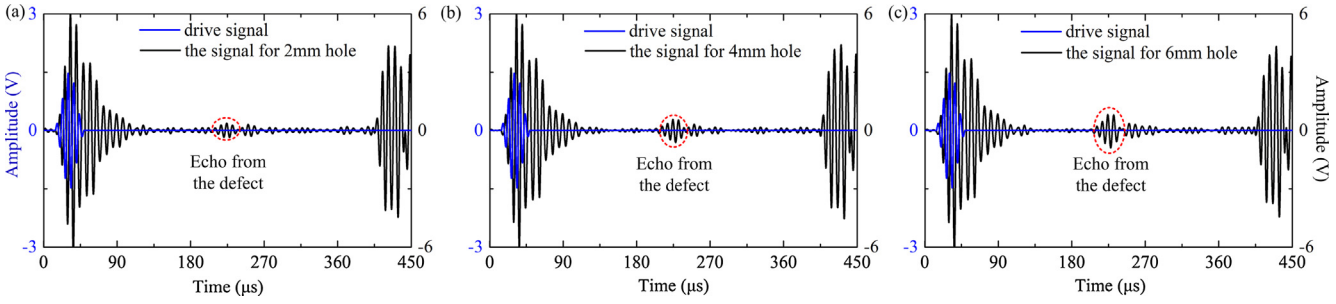

Fig. 7. The comparison of the reconstructed signal for the through-thickness hole with diameter of (a) 2 mm, (b) 4 mm and (c) 6 mm at 145 kHz.

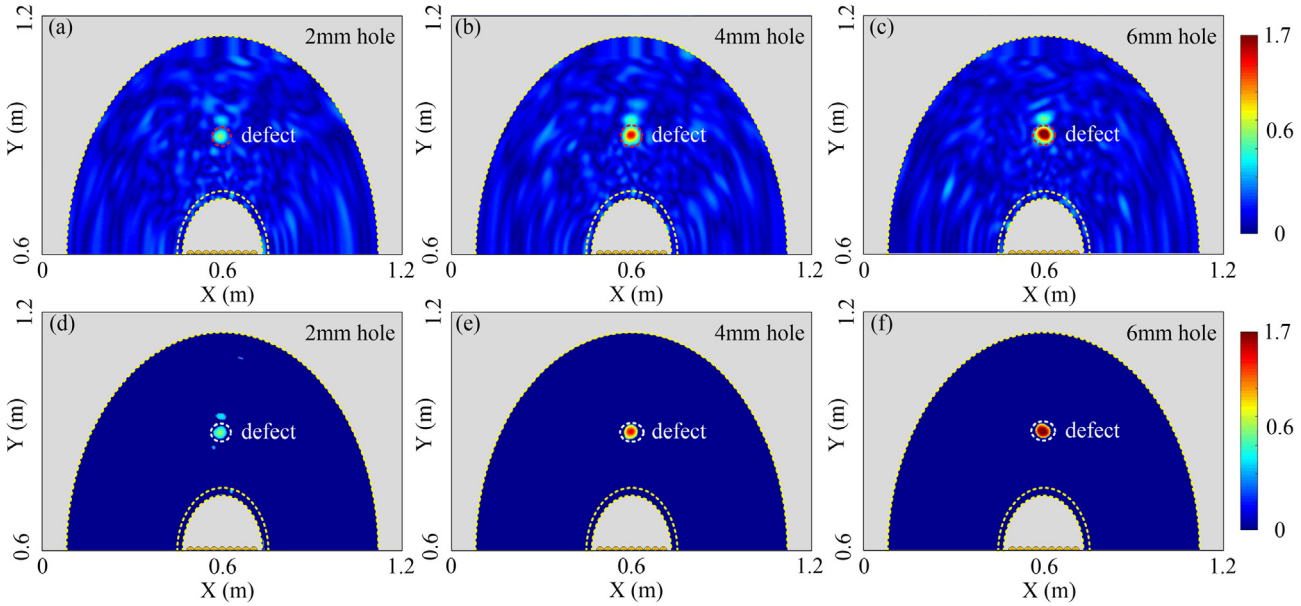

Fig. 8. The imaging results for the through-thickness hole with the diameter of 2 mm (left), 4 mm (middle) and 6 mm (right) at 145 kHz. Up: Original results. Bottom: Results after threshold truncation (50% of the maximum amplitude).

Table 1
The location results for the through-thickness hole with different size at 145 kHz.

Defect size (mm)	2	4	6
Actual position (mm)	(600, 900)	(600, 900)	(600, 900)
Located position (mm)	(606, 898)	(595, 901)	(599, 898)

4.3. Multiple through-thickness defects

Finally, the capacity of the proposed phased array system in multi defects detection was examined. Besides the 6 mm hole at 90° direction with the distance of 300 mm, another 6 mm through-thickness hole was introduced on the plate at 60° direction with the distance of 350 mm. Fig. 10(a) and (b) presented the reconstructed signals at 60° and 90° direction, respectively. In each figure, only one wave package appeared which corresponds to the echo from the defect. This result indicated that the proposed system can detect two defects simultaneously. Note that the echo amplitude for the defect at 60° direction was smaller than that at 90° direction. This may be caused by many factors such as varied reflectivity along different reflection paths, larger energy dissipation for longer propagating distance, deviation of beamforming, etc. In comparison with the single defect case, the noise amplitude of the reconstructed signals for two-defects case was somewhat enhanced, which should be attributed to the interactions of the reflected signals from the two defects since they are not far from each other. From the results in Fig. 10, it can be inferred that even using the phased array system, it is more difficult to detect multiple defects than single defect.

Fig. 11(a) and (b) presented the original imaging result and result after 50% threshold truncation at 145 kHz for the two through-thickness holes with the diameter of 6 mm. It can be seen that there only appeared two highlight areas which correspond to the two defects. This result further confirmed that the proposed SH_0 wave phased array system can detect multi defects simultaneously. The location results for the two defects were listed in Table 2, from which it can be seen the location error for Defect 1 turns to be 2.8 mm and that for Defect 2 is 6.4 mm, both larger than the single-defect case of 2.2 mm. This should also be attributed to the interactions between the reflected signals from the two defects. Nevertheless, such level of location accuracy is quite good considering its large inspection area.

It should be noted that at 145 kHz, the wavelength (λ) of SH_0 wave is 21.4 mm. The element spacing of 15 mm is about 0.7 λ. If the drive signal was continuous waveform, for the hole at 60° direction, there should appear a grating lobe (large artifact) around 160° direction. While it can be seen from Fig. 11(a) that there is no grating lobes at all, which may imply that the employed drive signal of five-cycle Hanning window-modulated sinusoid tone burst is fairly effective in suppressing

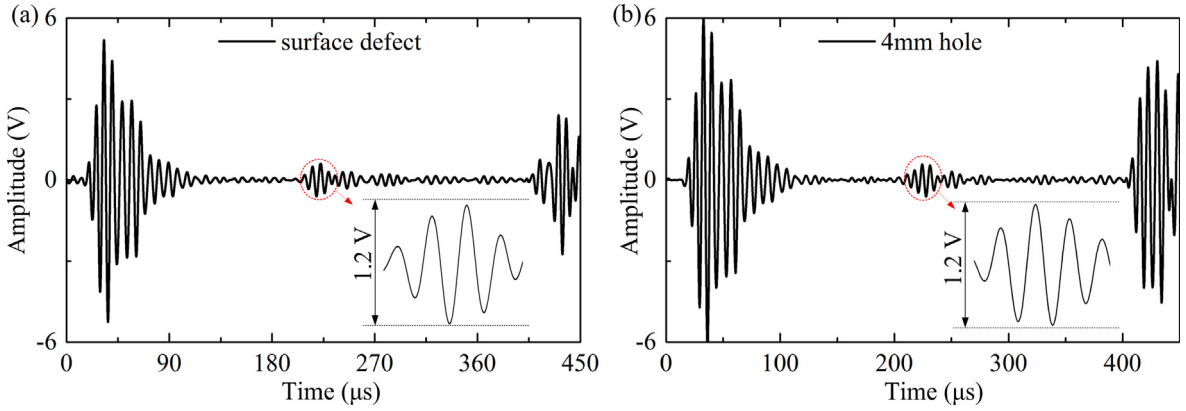

Fig. 9. The comparison of the reconstructed signals for (a) the bonded 20 mm-diameter iron rod and (b) 4 mm-diameter through-thickness hole at 145 kHz.

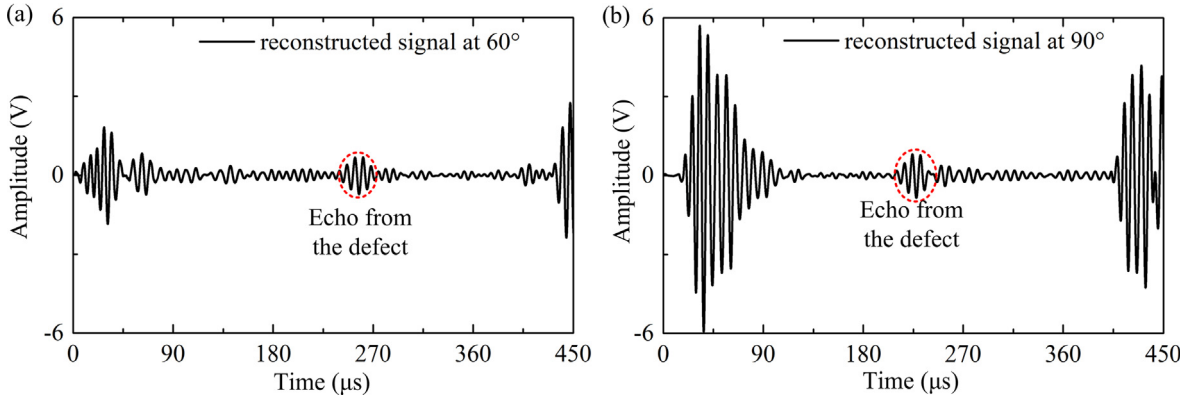

Fig. 10. The reconstructed signals at 145 kHz for two through-thickness holes with the same diameter of 6 mm at (a) 60° direction and (b) 90° direction.

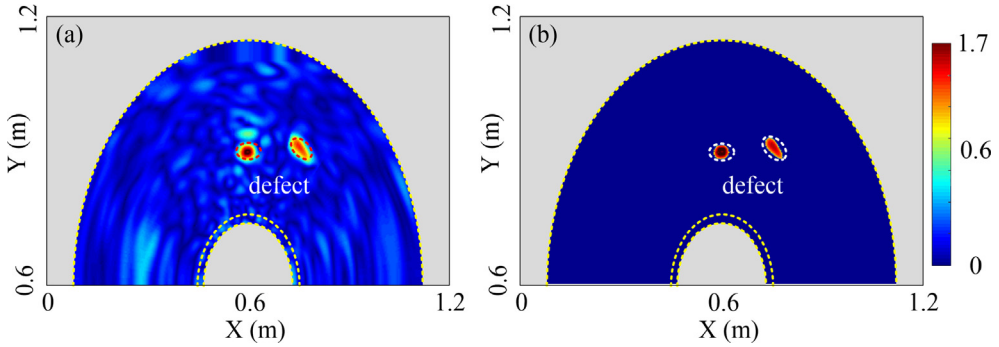

Fig. 11. The imaging results at 145 kHz for the two through-thickness holes with the same diameter of 6 mm. (a) Original results. (b): Results after threshold truncation (50% of the maximum amplitude).

Table 2
The location results for multi defects detecting at 145 kHz.

Defect number	D_1	D_2
Actual position (mm)	(600, 900)	(775, 903)
Located position (mm)	(598, 898)	(771, 908)

the grating lobes [33].

5. Conclusions

In this work, we proposed a linear phased array system for structural health monitoring (SHM) using omni-directional SH_0 wave piezoelectric transducers based on parallel ray approximation. The performance of the phased array system in damage detecting was systematically examined. Results indicated that it can detect both surface defects and through-thickness defects accurately at varied frequencies. Moreover, it has high resolution which can successfully detect a through-thickness hole as smaller as 2 mm in diameter. Besides, it can also detect multiple defects simultaneously. The good performance of this SHM system was mainly benefited from the employed non-dispersive SH_0 wave. Considering its simple structure and desirable results, this work is expected to lay the foundation of SH_0 wave based phased array SHM.

It should be noted that the mirror artifact is the inherent problem of the linear phased array system. Meanwhile, the parallel ray approximation used in this work makes the invalid near-field zone fairly large. In our ongoing work, two-dimensional phased array system is under development to remove the mirror artifact and exact wave path will be used to minimize the near field zone.

Acknowledgement

This work is supported by the National Natural Science Foundation of China under Grant No. 11672003.

Appendix A. Supplementary material

Supplementary data to this article can be found online at https://doi.org/10.1016/j.ultras.2019.04.005.

References

[1] F.-K. Chang, Structural Health Monitoring 2000, CRC Press, 1999.
[2] K. Diamanti, C. Soutis, Structural health monitoring techniques for aircraft composite structures, Prog. Aerosp. Sci. 46 (2010) 342–352.
[3] A.K. Jardine, D. Lin, D. Banjevic, A review on machinery diagnostics and prognostics implementing condition-based maintenance, Mech. Syst. Signal Process. 20 (2006) 1483–1510.
[4] V. Giurgiutiu, Structural Health Monitoring with Piezoelectric Wafer Active Sensors: With Piezoelectric Wafer Active Sensors, Elsevier, 2007.
[5] Y. Lu, L. Ye, Z. Su, Crack identification in aluminium plates using Lamb wave signals of a PZT sensor network, Smart Mater. Struct. 15 (2006) 839.
[6] X. Chen, J.E. Michaels, T.E. Michaels, A methodology for estimating guided wave scattering patterns from sparse transducer array measurements, IEEE Trans. Ultrason. Ferroelectr. Freq. Control. 62 (2015) 208–219.
[7] J. He, F.-G. Yuan, A quantitative damage imaging technique based on enhanced CCRTM for composite plates using 2D scan, Smart Mater. Struct. 25 (2016) 105022.
[8] J.E. Michaels, T.E. Michaels, Guided wave signal processing and image fusion for in situ damage localization in plates, Wave Motion. 44 (2007) 482–492.
[9] Z. Liu, F. Yu, R. Wei, C. He, B. Wu, Image fusion based on single-frequency guided wave mode signals for structural health monitoring in composite plates, Mater. Eval. 71 (2013).
[10] Z. Li, S. Xia, J. Wang, X. Su, Damage detection of cracked beams based on wavelet transform, Int. J. Impact Eng. 32 (2006) 1190–1200.
[11] J.E. Michaels, Detection, localization and characterization of damage in plates with an in situ array of spatially distributed ultrasonic sensors, Smart Mater. Struct. 17 (2008) 035035.
[12] T. Clarke, F. Simonetti, P. Cawley, Guided wave health monitoring of complex structures by sparse array systems: influence of temperature changes on

performance, J. Sound Vib. 329 (2010) 2306–2322.
[13] A.C. Clay, S.-C. Wooh, L. Azar, J.-Y. Wang, Experimental study of phased array beam steering characteristics, J. Nondestruct. Eval. 18 (1999) 59–71.
[14] S.-C. Wooh, Y. Shi, A simulation study of the beam steering characteristics for linear phased arrays, J. Nondestruct. Eval. 18 (1999) 39–57.
[15] P.D. Wilcox, Omni-directional guided wave transducer arrays for the rapid inspection of large areas of plate structures, IEEE Trans. Ultrason. Ferroelectr. Freq. Control. 50 (2003) 699–709.
[16] V. Giurgiutiu, J. Bao, Embedded-ultrasonics structural radar for in situ structural health monitoring of thin-wall structures, Struct. Health Monit. 3 (2004) 121–140.
[17] L. Yu, V. Giurgiutiu, In situ 2-D piezoelectric wafer active sensors arrays for guided wave damage detection, Ultrasonics 48 (2008) 117–134.
[18] L. Yu, V. Giurgiutiu, In-situ optimized PWAS phased arrays for Lamb wave structural health monitoring, J. Mech. Mater. Struct. 2 (2007) 459–487.
[19] L. Yu, V. Giurgiutiu, Advanced signal processing for enhanced damage detection with piezoelectric wafer active sensors, Smart Struct. Syst. 1 (2005) 185–215.
[20] L. Yu, V. Giurgiutiu, Multi-mode damage detection methods with piezoelectric wafer active sensors, J. Intell. Mater. Syst. Struct. 20 (2009) 1329–1341.
[21] L. Yu, Z. Tian, Guided wave phased array beamforming and imaging in composite plates, Ultrasonics 68 (2016) 43–53.
[22] Z. Tian, L. Yu, X. Sun, B. Lin, Damage localization with fiber Bragg grating Lamb wave sensing through adaptive phased array imaging, Struct. Health Monit. (2018) 1475921718755572.
[23] J. He, C.A. Leckey, P.E. Leser, W.P. Leser, Multi-mode reverse time migration damage imaging using ultrasonic guided waves, Ultrasonics (2018).
[24] V. Giurgiutiu, Tuned Lamb wave excitation and detection with piezoelectric wafer active sensors for structural health monitoring, J. Intell. Mater. Syst. Struct. 16 (2005) 291–305.
[25] C.J. Borigo, S.E. Owens, J.L. Rose, Piezoelectric shear rings for omnidirectional shear horizontal guided wave excitation and sensing, US Patent (2018) No. 14878595.
[26] P. Belanger, G. Boivin, Development of a low frequency omnidirectional piezoelectric shear horizontal wave transducer, Smart Mater. Struct. 25 (2016) 045024.
[27] H. Miao, Q. Huan, Q. Wang, F. Li, A new omnidirectional shear horizontal wave transducer using face-shear (d24) piezoelectric ring array, Ultrasonics 74 (2017) 167–173.
[28] Q. Huan, H. Miao, F. Li, A uniform-sensitivity omnidirectional shear-horizontal (SH) wave transducer based on a thickness poled, thickness-shear (d15) piezoelectric ring, Smart Mater. Struct. 26 (2017) 08LT01.
[29] Q. Huan, H. Miao, F. Li, A variable-frequency structural health monitoring system based on omnidirectional shear horizontal wave piezoelectric transducers, Smart Mater. Struct. 27 (2018) 025008.
[30] Q. Huan, M. Chen, F. Li, A practical omni-directional SH wave transducer for structural health monitoring based on two thickness-poled piezoelectric half-rings, Ultrasonics 94 (2019) 342–349.
[31] C. Holmes, B.W. Drinkwater, P.D. Wilcox, Post-processing of the full matrix of ultrasonic transmit–receive array data for non-destructive evaluation, NDT&E Int. 38 (2005) 701–711.
[32] D.H. Johnson, D.E. Dudgeon, Array Signal Processing: Concepts and Techniques, PTR Prentice Hall, Englewood Cliffs, 1993.
[33] B.W. Drinkwater, P.D. Wilcox, Ultrasonic arrays for non-destructive evaluation: a review, NDT&E Int. 39 (2006) 525–541.
[34] E. Leinov, M.J. Lowe, P. Cawley, Ultrasonic isolation of buried pipes, J. Sound Vib. 363 (2016) 225–239.